Calibration-Free Measurement of Liquid Permittivity and Conductivity Using Electrochemical Impedance Test Cell With Servomechanically Adjustable Cell Constant

Hongshen Ma, *Member, IEEE*, Jeffrey H. Lang, *Fellow, IEEE*, and Alexander H. Slocum

***Abstract*—This paper presents a technique and a device for measuring the permittivity and conductivity of liquids and gases that does not require prior calibration by a reference sample. The technique involves precisely controlling the separation between two closely spaced spherical electrodes to make electrical impedance measurements of the sample media as a function of electrode separation. By leveraging the geometrical accuracy of the spheres and precise control of the electrode separation, the permittivity and conductivity of the sample can be extracted using a simple geometrical model of the electrode. Calibration using a reference sample is replaced by mechanical calibration of the sphere diameter and separation control mechanism, which can be engineered simply and accurately using standard components and processes. The electrode separation is adjusted using a flexure stage and a servomechanical actuator, which enables control of the electrode separation with 0.25 nm resolution with a 50 μm range. Permittivity and conductivity measurements within 1% of established values have been demonstrated.**

***Index Terms*—Calibration-free measurements, conductivity, electrochemical impedance, permittivity, water purity.**

I. Introduction

ELECTRICAL permittivity and conductivity are fundamental physicochemical properties of liquids. In solutions, permittivity is a measure of the polarizability of the solvent, while conductivity is a measure of the concentration and mobility of the solute. Applications of permittivity measurements include determining the composition of solvents in solution chemistry [1], [2], soil moisture content in geological survey [3], and liquid-gas fraction in chemical processing [4], [5]. Applications of conductivity measurements include determining contaminant levels in drinking water, boiler water purity in power plants [6], health of lubrication oils in heavy machinery [7], performance of battery electrolyte [8], and concentration of chemical products in microfludic analysis systems [9]. Electrical conductivity of liquids can also be used to detect the presence of specific chemicals if coupled with enzymatic assays designed to produce conductiometric readout [10].

Accurate and repeatable permittivity and conductivity measurements are key requirements of sensor systems that utilize this mode of detection. Since permittivity and conductivity, ε and κ, are intensive parameters, they must be derived from the measurable quantities of capacitance and conductance, C and G, using a geometrical model of the impedance test cell described by the cell constant, K_{cell}. These quantities are related by the following equations:

$$C = \frac{\varepsilon}{K_{\text{cell}}} + C_0. \tag{0.1}$$

$$G = \frac{\kappa}{K_{\text{cell}}} + G_0 \tag{0.2}$$

where the capacitance C_0 and conductance G_0, are parasitic values not included in the model for K_{cell}.

While the values of capacitance and conductance can be measured with a high degree of accuracy, the variability of K_{cell}, C_0, and G_0 can result in inaccuracies in ε and κ. Since C_0 and G_0 depend on the detailed geometry of the electrodes and their manufacturing process, the values of these terms cannot be easily predicted. As a result, determining ε and κ based on a geometrical model of K_{cell} is extremely difficult. The addition of guard electrodes can reduce the value of C_0 and G_0, but not eliminate them completely. Surface properties such as electrode polarization [11], corrosion, and absorption, can produce additional errors by altering the size of the impedance test cell. In portable and/or low-cost analysis systems with limited sample volume, the effect of these aforementioned errors may be further exaggerated, thus nullifying the use of these systems to measure ε and κ.

Existing conductivity meters typically address the uncertainty of K_{cell} by periodically calibrating the impedance test cell using a standard solution with established values of ε and κ. This correction is of limited value since K_{cell}, C_0 and G_0 can also be dependent on the value of ε and κ. As a result, the calibration

Manuscript received June 08, 2008; revised September 02, 2008; accepted September 05, 2008. Current version published March 27, 2009. This research was supported in part by MIT's Center for Bits and Atoms under NSF Grant CCR-0122419). An earlier version of this paper was presented at the 2007 IEEE Sensors Conference and was published in its proceedings. Any opinions, findings, and conclusions or recommendations expressed in this paper are those of the authors and do not necessarily reflect the views of the NSF. The associate editor coordinating the review of this paper and approving it for publication was Prof. Evgenty Katz.

H. Ma and A. H. Slocum are with the Department of Mechanical Engineering, Massachusetts Institute of Technology, Cambridge, MA 02139 USA (e-mail: hongma@alum.mit.edu; slocum@mit.edu).

J. H. Lang is with the Department of Electrical Engineering and Computer Science, Massachusetts Institute of Technology, Cambridge, MA 02139 USA (e-mail: lang@mit.edu).

Color versions of one or more of the figures in this paper are available online at http://ieeexplore.ieee.org.

Digital Object Identifier 10.1109/JSEN.2009.2015401

is valid only when ε and κ of the sample and calibration fluid are within a narrow range of one another [7], [8]. The use of calibration liquids is also often impractical since the calibration liquid may irreversibly contaminate the impedance test cell.

Accurate measurement of permittivity and conductivity without wet calibration can be made using impedance test cells where the cell constant can be adjusted in a predictable manner. A variable cell constant could be implemented by either adjusting the separation between the electrodes or the electrode overlap area. The former technique have been used by Barthel [12], [13] and by Wu [14] to obtain standard reference values for permittivity and conductivity [15], [16]. These devices encapsulate sample media in a glass cylinder with platinum electrodes mounted on the end of the cylinder. The cylinder contains a removable section of a precisely measured length. The differential capacitance and conductance measured with and without the middle section is used to compute the absolute permittivity and conductivity.

A simpler method for adjusting the cell constant was developed by Shiefelbein [8], which consists of an inner rod electrode concentric with an outer cylindrical electrode. By varying the level of immersion of the electrode in the sample media, the absolute value of permittivity and conductivity can be extracted from the differential values of capacitance and resistance. Using this apparatus, Shiefelbein demonstrated that the conductivity of KCl solutions could be measured to within 1% of standard reference values.

The design of impedance test cells with an adjustable cell constant highlights a fundamental tradeoff between varying the cell constant over a range sufficient to make an accurate estimate of the permittivity and conductivity, while minimizing the variation of parasitic capacitance and conductance. This tradeoff can be optimized at small electrode separations because small modulations of the electrode separation result in large variations of the cell constant, while the corresponding variations of parasitic capacitance and conductance are minimized. In the development of portable chemical analysis systems, where a conductivity assay may be used to detect the presence of target chemicals, small gap electrode geometries are also advantageous for reducing the volume of reactants, and correspondingly, the total cost of analysis.

The design of impedance test cells with small, adjustable electrode separations between planar electrodes has many practical challenges since parallelism errors between the electrodes can produce large offsets in the measured result. The design for such apparatuses for permittivity and conductivity measurements has been explored without success using the apparatus of White [17] and the apparatus of Wu [18]. The parallelism problem can be avoided using spherical electrodes since the nearest points between two spheres are by definition tangential. (This principle is similarly true for the geometry of a sphere and a plane.) Additionally, spheres can be inexpensively manufactured with high diametrical accuracy and extremely smooth surfaces. For polished spheres that are a few millimeters in diameter, the diametrical tolerance can typically be less than one micrometer, while the RMS surface roughness can be as low as a few nanometers.

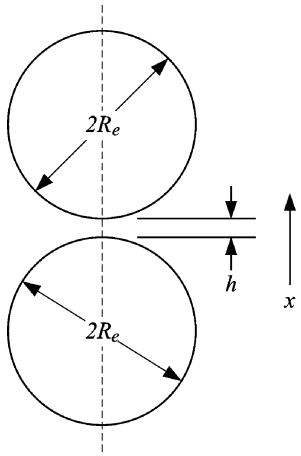

Fig. 1. Electrostatic model.

The technique presented in this paper leverages the diametrical tolerance of a sphere and precise adjustment of the electrode separation to enable accurate measurement of permittivity and conductivity. The wet calibration required in previous devices is replaced by mechanical calibration of the sphere diameter and separation control mechanism, which can be engineered simply and accurately using standard components and processes. The concept for this device and its demonstration on permittivity measurements has been described in an earlier publication [19]. This paper describes the detailed design of the device and demonstrates its use for conductivity measurements [20].

II. Theory

A. Electrostatic Model

The capacitance C between two perfectly conducting spheres, in a uniformally polarizable media, shown in Fig. 1, has the exact expression [21]

$$C = 2\pi R_e \varepsilon_r \varepsilon_0 \sinh(\alpha) \sum_{n=1}^{+\infty} \frac{1}{\sinh(n\alpha)} \tag{1.1}$$

$$\cosh(\alpha) = 1 + h/2R_e \tag{1.2}$$

where R_e is the radius of the spheres, ε_0 is the vacuum permittivity, ε_r is the relative permittivity, and h is the distance between the electrodes measured from their nearest points. When the two electrodes are extremely close to one another, i.e., $h \ll R_e$, the following approximate expression:

$$C = \pi R_e \varepsilon_r \varepsilon_0 \ln\left(\frac{2R_e}{h}\right) + C_1 \tag{1.3}$$

derived by Boyer [21], could be used, where C_1 is a constant. This expression has the characteristic that the spatial derivative of C is inversely proportional to h such that

$$\left(\frac{dC}{dh}\right)^{-1} = -\frac{h}{\pi R_e \varepsilon_r \varepsilon_0}. \tag{1.4}$$

Thus, using the capacitance measured at several values of h, it is therefore possible to extract the value of ε_r. Furthermore, since the physical laws governing conductance are exactly parallel to

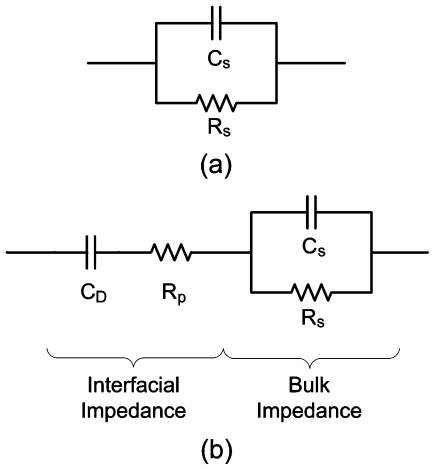

Fig. 2. Equivalent circuit representations of: (a) uniformally polarizable media and (b) media with mobile charge carriers.

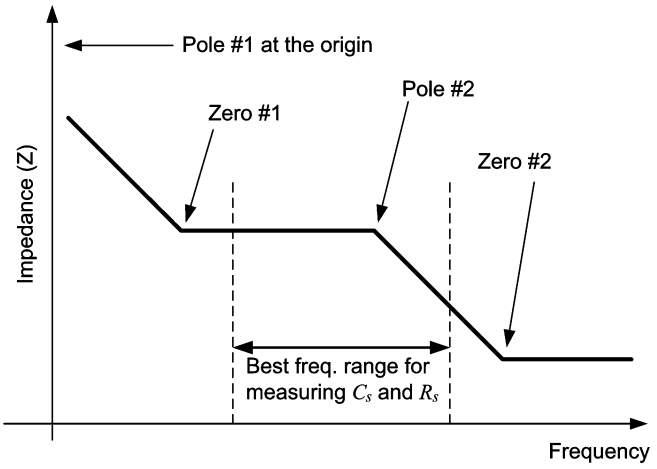

Fig. 3. Bode plot of the equivalent circuit of an impedance cell containing mobile charge carriers.

capacitance, the relationship between conductance and conductivity obey the expression

$$G = \pi R_e \kappa \ln\left(\frac{2R_e}{h}\right) + G_0 \tag{1.5}$$

which correspondingly gives

$$\left(\frac{dG}{dh}\right)^{-1} = -\frac{h}{\pi R_e \kappa}. \tag{1.6}$$

B. Electrochemical Model

Uniformally polarizable media without mobile charge carriers such as air and hexane can be modeled using a simple equivalent circuit consisting of a capacitor C_s, and a resistor R_s in parallel, as shown in Fig. 2(a). Sample media with mobile charges, such as water and alcohols form an electrical double layer at the electrode-electrolyte interface. The electrical properties of the double layer in the non-faradic regime can be approximately described using the Gouy–Chapmann–Stern (GCS) model [22]. While the validity of this model has recently been called into question [23], for the purpose of measuring properties of the bulk liquid independent of surface layer effects, it is sufficient to approximate this region using the equivalent circuit model shown in Fig. 2(b). The effect of the double layers on both electrodes is represented using the series circuit elements C_p and R_p. Physically, C_p represents the buildup of charge in the double layer, while R_p represents conductivity of the interfacial region resulting from this accumulation of charge. The lack of a DC conductance path in this model is an artifact of a *blocking*, or nonreactive, electrode that does not permit direct transport of electrons from the electrode and the solution. The impedance of the circuit in Fig. 2(b) is

$$Z = \frac{R_s}{1 + j\omega R_s C_s} + R_p + \frac{1}{j\omega C_p}. \tag{1.7}$$

Combining the terms into one fraction (1.7), becomes

$$Z = \frac{-\omega^2 R_s C_s R_p C_p + j\omega(R_s C_s + R_p C_p + R_s C_p) + 1}{j\omega C_p(1 + j\omega R_s C_s)} \tag{1.8}$$

which can be expressed as

$$Z = \frac{R_s C_s R_p C_p (j\omega + \omega_{Z1})(j\omega + \omega_{Z2})}{j\omega C_p(1 + j\omega R_s C_s)} \tag{1.9}$$

Equation (1.9) has a pole at the origin, a second pole at a higher frequency, and two zeros. A Bode plot of the impedance is shown in Fig. 3. The pole at the origin arises from the capacitor C_p, while the second pole arises from the time constant of the bulk liquid defined by the elements, C_s and R_s. The frequency of this pole ω_{P2} is intrinsic to the sample media since

$$\omega_{P2} = \frac{1}{R_s C_s} = \frac{\kappa}{\varepsilon}. \tag{1.10}$$

Thus, in order to obtain precise measurements of ε and κ in the frequency domain, it is important to excite the system near this frequency. For aqueous solutions at room temperature, the value of ε is expected to be approximately $80\varepsilon_0$, while the value of κ is expected to range between 10^{-6} S/m and 0.1 S/m. The frequency of ω_{P2} will therefore range from approximately 220 Hz to 22 MHz.

The expression for the zeros of (1.9), ω_{Z1} and ω_{Z2}, can be determined to be (1.11) shown at the bottom of the page. An approximate expression for the lower frequency zero, ω_{Z1}, as

$$\omega_{Z1,Z2} = \frac{(R_s C_s + R_p C_p + R_s C_p) \mp \sqrt{(R_s C_s + R_p C_p + R_s C_p)^2 - 4R_s C_s R_p C_p}}{2R_s C_s R_p C_p} \tag{1.11}$$

a function of its dominant terms can be obtained by rewriting (1.11) as

$$\omega_{Z1} = \frac{p}{q}\left(1 - \sqrt{1 - \frac{2q}{p^2}}\right) \tag{1.12}$$

where

$$p = R_s C_s + R_p C_p + R_s C_p \tag{1.13}$$
$$q = 4 R_s C_s R_p C_p. \tag{1.14}$$

Expression (1.11) can be rewritten again as the series expansion

$$(1+\alpha)^n = 1 + n\alpha + \frac{n(n-1)}{2!}\alpha^2 + \ldots \tag{1.15}$$

where

$$\alpha = -\frac{2q}{p^2} \text{ and } n = \frac{1}{2}. \tag{1.16}$$

Taking the first two terms of the series yields an approximate expression for ω_{Z1}

$$\omega_{Z1} \approx \frac{1}{p} = \frac{1}{(R_s C_s + R_p C_p + R_s C_p)}. \tag{1.17}$$

This expression is a rather intuitive result, which says that the value of ω_{Z1} is determined by the time constant of the bulk impedance, the time constant of the interfacial impedance, and the time constant that describes the interaction between these two components. Expressions (1.10) and (1.17) indicate that the frequency of ω_{Z1} is lower than that of ω_{P2} and thus validating the Bode plot in Fig. 3.

An approximate expression can also be derived for the higher frequency zero, ω_{Z2}. Since it can be shown that

$$(R_s C_s + R_p C_p + R_s C_p)^2 \gg 4 R_s C_s R_p C_p \tag{1.18}$$

the second term under the square root in (1.11) can effectively be neglected. The expression for ω_{Z2} can thus be approximated as

$$\omega_{Z2} \approx \frac{(R_s C_s + R_p C_p + R_s C_p)}{R_s C_s R_p C_p}. \tag{1.19}$$

The expressions for ω_{Z1} and ω_{Z2} can be further simplified by comparing the terms of $R_s C_s + R_p C_p + R_s C_p$. Since the electrode separation is generally much greater than the effective length of the interfacial layer, which is characterized by the Debye length and is typically no more than 100 nm, it can be assumed that $R_s \gg R_p$ and $C_p \gg C_s$. Therefore, it can be assumed $R_p C_p + R_s C_p \approx R_s C_p$ and $R_s C_s + R_s C_p \approx R_s C_p$. As a result, the expressions for ω_{Z1} and ω_{Z2} can be written as

$$\omega_{Z1} \approx \frac{1}{R_s C_p} \tag{1.20}$$
$$\omega_{Z2} \approx \frac{1}{C_s R_p}. \tag{1.21}$$

Reapplying the previous argument yield the results

$$\omega_1 < \frac{1}{R_s C_s} \text{ and } \omega_2 > \frac{1}{R_s C_s}. \tag{1.22}$$

It should be noted, however, that in situations where the electrode separation is less than or approximately equal to the Debye length, these assumptions no longer hold, and more sophisticated models are required to interpret the measured impedance.

III. Device Design

A. Electrode

The spherical electrodes are fabricated using silicon-nitride spheres as the substrate for a thin platinum film. Traditionally used in low-friction bearings and precision alignment equipment, silicon-nitride spheres have exceptional dimensional accuracy, mechanical stiffness, surface quality, and stability over temperature.

The spheres used to fabricate the electrode have a diameter of 9.5252 mm with a tolerance of $\pm 0.25\ \mu$m (Cerbec Saint Gobain Ceramics: Grade 5 spheres). The surface quality of the spheres has been analyzed using a whitelight profilometer (Zygo), which showed a surface roughness of 2 nm RMS and the peak-to-valley range of approximately 50 nm. For comparison, polished silicon wafers analyzed using the same instrument showed a surface roughness of 1 nm RMS and a peak-to-valley range of 20 nm.

The electrode film consists of a 50 nm platinum layer and a 5 nm chromium adhesion layer. The metal films are deposited on one hemisphere of the silicon-nitride spheres using electron-beam deposition. Further surface analysis confirmed that the electrode films coat the silicon-nitride spheres conformally and does not change its surface roughness characteristics.

As Section V will show, while this choice of electrode materials is sufficient for permittivity measurements, the corresponding conductivity measurement showed a slow increase over time, which is likely caused by dissimilar metal contacts between the sphere and its mechanical mount. This problem has been resolved using ANSI-316 stainless-steel spheres to match the metal used to fabricate the mounting structure for the electrode.

B. Impedance Test Cell

The electrodes are mechanically constrained in a cylindrical bore on the tip of a 12.7 mm diameter, ANSI-316 stainless-steel shaft. An externally threaded ring nut constrains the electrode sphere inside the bore with only a small region protruding, as shown in Fig. 4. Two dimples on the ring nut allow it to be tightened using a custom-made wrench. When tightened, the ring nut bends slightly and applies a mechanical preload to the electrode to ensure that the electrode and shaft are tightly bound together. Mechanical contact between the ring nut and the electrode also serves as the electrical contact between the platinum film and the mounting shaft. Therefore, the mounting shaft becomes part of the electrode for measuring impedance. The addition of the electrode mounting structure introduces an error to the shape of the electrodes. However, since most of the electric energy is concentrated in the small gap region between the electrodes, the effect of this error is minimal if measurements are made at small electrode gaps.

The electrode separation is modulated by precise adjustment of the position of the mounting shafts using a flexural stage.

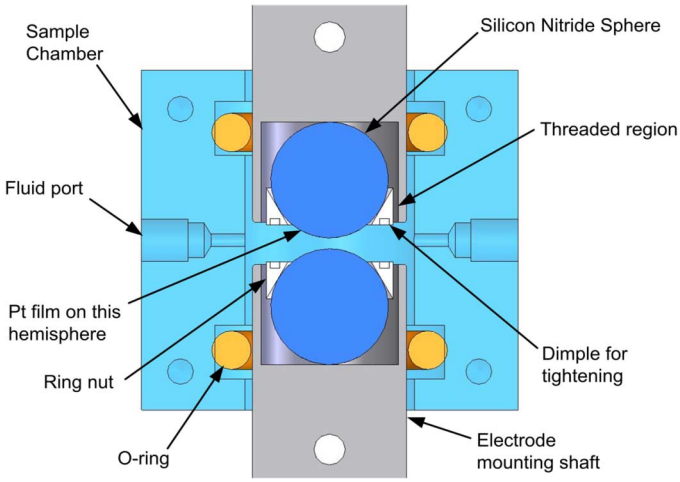

Fig. 4. Cross section of the electrode mount and the sample chamber.

The two mounting shafts are aligned in the flexure mechanism, but are electrically isolated from the mechanism via a 50 μm layer of polyimide film (McMaster: 2271K72). The displacements of both mounting shafts are measured using capacitance probes (Lion precision) pointed at the end of the shaft as shown in Fig. 5. Grounded target electrodes epoxied to the end of each shaft prevent the capacitance probe from interfering with the impedance measurement.

The sample chamber is designed to constrain the sample fluid between the electrodes while allowing small modulations of the electrode separation. As shown in Figs. 4 and 7, the sample chamber is approximately a cube with a central bore for the mounting shafts. The sample chamber is fabricated using ANSI-316 stainless steel with external dimensions of $27.9\ \mathrm{mm} \times 30.5\ \mathrm{mm} \times 25.4\ \mathrm{mm}$. A liquid seal is established between each mounting shaft and the sample chamber via a Kalrez O-ring (-206 Dupont compound 4079), which has properties similar to Teflon, but with significantly greater elasticity.

It is important to note that when the electrode separation is adjusted over the designed range of 50 μm, the O-ring does not slip against the mounting shaft or the O-ring grooves in the sample chamber. Rather, the O-rings act as elastic elements (flexures) that enable this deflection by shear strain. As a result, the motion of the shaft is mechanically repeatable and does not suffer from hysteric errors inherent in sliding contacts.

Liquid samples are introduced into the sample chamber via fluidic ports for 1/16-inch OD tubing (Upchurch: M-644-03), connected to a standard syringe. The inlet port is located near the bottom of the chamber while the outlet port is located near the top in order to prevent air bubbles from accumulating in the chamber. The chamber also contains a window for debugging purposes. This window is covered with a 3-mm-thick round Pyrex window (Esco products: P705125), which is also sealed using a Kalrez O-ring.

C. Positioning Mechanism

The positioning mechanism, shown in Fig. 6, is a 6061 T651 aluminum monolith consisting of three main functional groups: coarse adjustor; fine adjustor; and metrology frame. The electrode mounting shafts are constrained to the aluminum monolith using a semicircular clamp, as shown in Fig. 7. The top shaft is connected with a symmetric dual beam flexure, which is part of the fine actuator. The bottom shaft is not rigidly clamped when the coarse adjustor is active, but once the desired position has been reached, this shaft is similarly fixed via a semicircular clamp.

The coarse adjustor sets the initial separation of the electrodes to within range of the fine adjustor. This mechanism consists of an ultra fine thread lead screw (Thorlabs: 1/4″-80 screw FS25AB200), shown in Fig. 7, that advances the bottom mounting shaft. The positioning accuracy is enhanced by an anti-backlash bushing which applies a consistent preload to the screw. Assuming 1° angular resolution is achievable by hand, the position of the electrode can be advanced with a resolution of 0.3 μm. In order to prevent the lead screw from deforming the flat surface, a steel puck with one flat and one conical surface is added to the interface between the spherical tip on the lead screw and the flat surface of the mounting shaft.

The coarse adjustor is mounted on a separate aluminum block that can be detached from the main frame. Once the desired electrode position has been reached, the bottom mounting shaft can be rigidly clamped to the frame. The coarse adjustor can then retracted and replaced by a capacitance probe that measures the displacement of the bottom mounting shaft. The removable coarse adjustor reduces the complexity of having to measure and deflect the same surface.

The fine adjustor is designed to control the position of the top electrode mounting shaft with nanometer accuracy from a servomechanical actuator. There are four main components in this mechanism: symmetric dual beam flexure, wobble pin, cantilever beam, and the linear servo actuator.

The symmetric dual beam flexure constrains the displacement of the top shaft along the vertical direction with high mechanical impedance. The ratio of the stiffness of this flexure relative to that of the cantilever beam acts to demagnify the displacement of the actuator with a high transmission ratio. The stiffness of this flexure is controlled by the length and width of the flexure beams. These dimensions are chosen to maintain maximum stiffness, while staying within the load capabilities of the actuator.

A common problem in high transmission ratio flexure mechanisms is the presence of parasitic displacement along orthogonal axes. In order to constrain displacement of the top shaft along the x axis, while reducing parasitic displacement along the y and z axes, a wobble pin is used to transfer displacement from the cantilever beam to the symmetric dual beam flexure. Instead of a standalone pin assembled between the transducer and the end-effector to only transmit axial forces [24], the wobble pin used here is monolithic with the rest of the flexure and consists of two thin flexure beams. The two-prong design provides the flexibility desired in a wobble pin with the capability of integrating a capacitance probe through its center. The two-prong flexure beams are manufactured by first drilling a center hole in the flat aluminum stock, and removing a small amount of material away from the exterior faces, before using a Waterjet Machining Center (OMax) to make the final cut.

The cantilever beam reduces the displacement from the actuator to the symmetric dual beam flexure. A tapered single-beam design efficiently distributes stress along the length of the beam. The transmission ratio is set by the relative stiffness of the

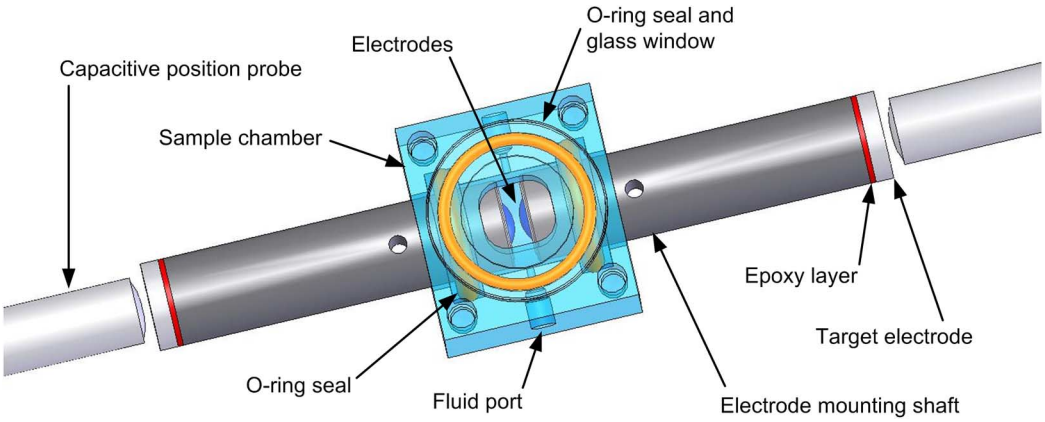

Fig. 5. Design of the impedance cell.

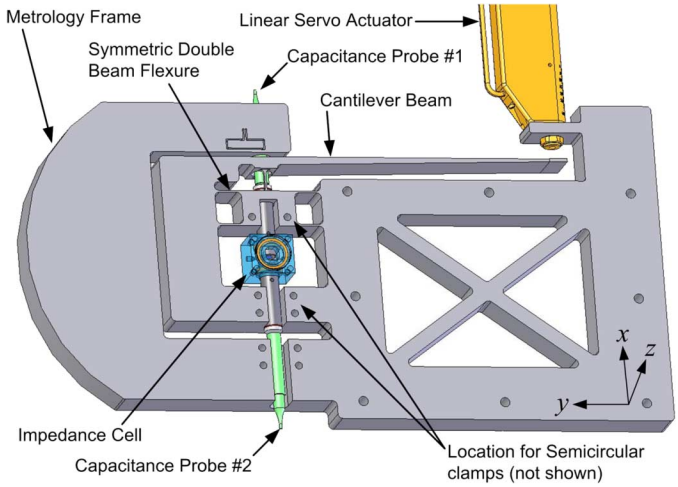

Fig. 6. The mechanism for adjusting the electrode separation.

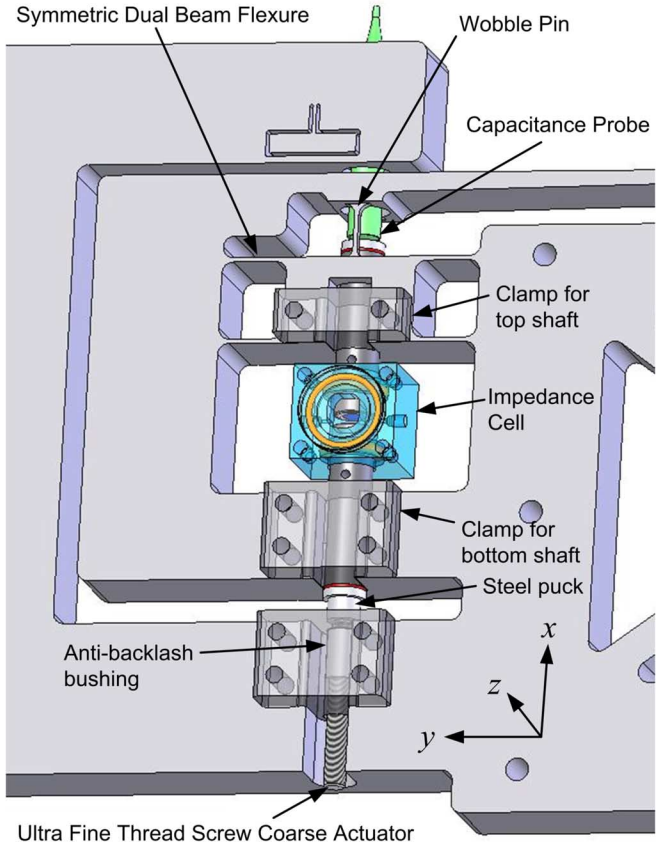

Fig. 7. Close up of the adjustment mechanism.

symmetric dual beam flexure and the stiffness of the cantilever beam. These values are optimized using finite element analysis to set a transmission ratio of 200:1. The maximum deflection of the cantilever beam is designed to be 50% of the yield stress of 6061-T6 aluminum, which limits maximum deflection to be approximately 10 mm, corresponding to a maximum range of 50 μm. The range of the flexure is enforced using mechanical stops built into the structure of the flexure.

A linear actuator advances the electrode position by deflecting the tip of the cantilever beam. This actuator is a servomechanical leadscrew with feedback from an optical rotary encoder (Newport: LTA-HL). This actuator has a minimum incremental step of 50 nm and a 7 nm encoder resolution. Based on the designed 200:1 transmission ratio, this mechanism can be positioned in increments of 0.25 nm. The tip of the actuator is a nonrotating sphere, 6 mm in diameter. In order to ensure consistent contact between the actuator and the cantilever beam and prevent plastic deformation of the beam, a polished tungsten-carbide flat is added to the interface between the tip of actuator and the tip of the cantilever beam. The polished tungsten-carbide flat is found from a triangular lathe insert, and it is epoxied to the tip of the cantilever beam.

The displacements of both electrode mounting shafts are measured using capacitance probes (Lion Precision), as shown in Fig. 5. Grounded target electrodes are epoxied to the end of each electrode shaft in order to prevent the capacitance probe from interfering with the impedance measurement. The accuracy of these capacitance probes are specified with an RMS resolution of 0.2 nm at a bandwidth of 100 Hz. These probes are mounted in a metrology frame that is structurally isolated from the rest of the mechanism. The metrology frame is C-shaped, as opposed to an ideal closed shape. However, this is compensated by its robust size and integration with the aluminum monolith from which the entire device is constructed. The top probe reaches through a hole between the two flexures of the wobble pin. The diameter of the hole is greater than the diameter of

the probe in order to prevent the motion of the cantilever beam from displacing the probe. The sum of the readout from the capacitance probes gives a precise measurement of the change in the electrode separation. The two probe setup accounts for possible errors caused by the finite stiffness of the flexure frame and the connection between the electrode shaft and the frame.

D. Impedance Measurement

The interelectrode sample impedance is measured using an Agilent 4284A LCR meter, which uses an auto-balancing bridge circuit [25] to measure the complex impedance with a high degree of accuracy. This measurement configuration has the advantage that one measurement terminal is held at a virtual ground, which means that guard electrodes used to reduce the amount of stray impedance can simply be connected to the ground of the 4284A. For the apparatus described in this paper, both the sample chamber and the flexure mechanism are connected to ground to act as guard electrodes.

E. Data Acquisition and Temperature Control

Data acquired from the 4284A and the capacitive displacement probes are digitized and transmitted via GPIB to a PC where a Visual Basic program collects and stores the data. The entire apparatus is enclosed within a temperature-controlled chamber. The temperature inside the chamber is modulated using a radiator system fed by a circulating refrigerator (NESLab RTE). The temperature value could be adjusted within ± 10 °C from the ambient temperature.

IV. Analysis

An important property of this device is that the absolute electrode separation, h, cannot be measured directly. Instead, capacitance probes measure displacement along the x axis, which means that the value of h is known to within an offset x_0 such that $h = x - x_0$. The output value consists of ordered pairs of impedance values as a function of x. In the frequency range outlined in the electrochemical model of the system, the measured impedance could be separated into corresponding values of C and G which correspond to C_s and G_s (the reciprocal of R_s). The value of ε_r and κ can be extracted using the spatial derivatives of C and G, according to (1.4) and (1.6). Since data points are collected as discrete values, the value of the derivative can be estimated using the secant approximation where

$$\frac{dx}{dC} \approx \frac{x_{n+1} - x_n}{C_{n+1} - C_n}. \tag{3.1}$$

The Value of dx/dC is evaluated at the midpoint of x_n and x_{n+1}, and using the derivation for permittivity as an example, (1.4) becomes

$$-\pi R_e \varepsilon_0 \left(\frac{x_{n+1} - x_n}{C_{n+1} - C_n} \right) = \frac{(x_{n+1} - x_n)/2 - x_0}{\varepsilon_r}. \tag{3.2}$$

At this point, it is convenient to define a new variables u and v such that

$$u_n \equiv -\pi R_e \varepsilon_0 \left(\frac{x_{n+1} - x_n}{C_{n+1} - C_n} \right) \tag{3.3}$$

and

$$v_n \equiv -\pi R_e \left(\frac{x_{n+1} - x_n}{G_{n+1} - G_n} \right). \tag{3.4}$$

The permittivity can therefore be determined by a linear least squares fit of the ordered pairs of (x_n, u_n) to $u = a + bx$. As a result,

$$\varepsilon_r = \frac{1}{b} \text{ and } x_0 = \frac{x_{n+1} - x_n}{2} - a \cdot \varepsilon_r. \tag{3.5}$$

One of the underlying assumptions of least squares fitting is that the standard deviation of the variables is constant for all values. This assumption is violated for u, since u is a function of the differential values of x and C. At large electrodes separations, ΔC is relatively small, and this means that the standard deviation of ΔC, or σ_u is relatively large. At small electrode separations, the converse is true. Effects of the variable σ_u can be compensated using a weighted least squares (WLS) fitting. In the standard application of this technique, the weight function, w, is defined as the reciprocal of the variance of the data

$$w = 1/\sigma_u^2. \tag{3.6}$$

Assuming that the effect of the uncertainty in ΔC is much greater than the uncertainty of x, the weight function can be derived using standard statistical formulae as

$$w_n = \frac{1}{2\sigma_C^2} \left(\frac{\pi \varepsilon_0 R_e \ln\left(\frac{x_{n+1} - x_0}{x_n - x_0} \right)}{u_n} \right)^2. \tag{3.7}$$

Since the value of x_0 is initially unknown, an initial guess for x_0 can be obtained using a simple least squares fit. Estimates for x_0 can then be improved using iterative application of the WLS fitting procedure. Three iterations are typically sufficient for x_0 to converge to within 1 nm. The values for ε_r and κ can alternatively be extracted using direct nonlinear fitting to (1.3) and (1.5). However, these studies are less robust to noise than weighted least squares.

V. Results and Discussions

A. Electrical Permittivity Measurements

The operation of this device is initially characterized using dry nitrogen gas, which has a permittivity of 1.00 and negligible conductivity. These measurements are made starting at a large electrode gap, typically 10–15 μm, and decremented in steps of approximately 0.5 μm until the electrodes come into contact with one another. The sinusoidal excitation signal has an amplitude of 500 mV RMS, and a frequency of 120 kHz; 120 kHz is chosen because it is least affected by nearby electronic interference sources, such as the PWM signal from the servomechanical actuator.

Data from the nitrogen gas measurement are plotted in Fig. 8, where the electrode separation $x - x_0$ is plotted along the horizontal axis, while the transformed variable u is plotted along the vertical axis. The data points lie on a straight line, as predicted by (1.4). The measured relative permittivity is 1.007 ± 0.002, which is within 1% of the expected value for nitrogen gas. The

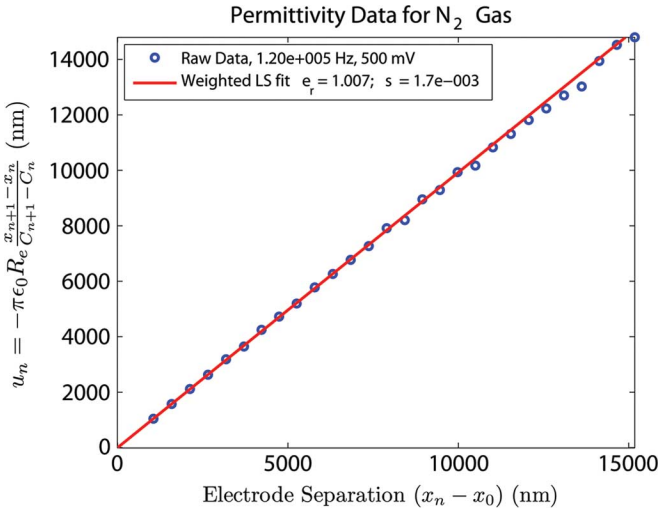

Fig. 8. Permittivity results for nitrogen gas transformed according to (3.3).

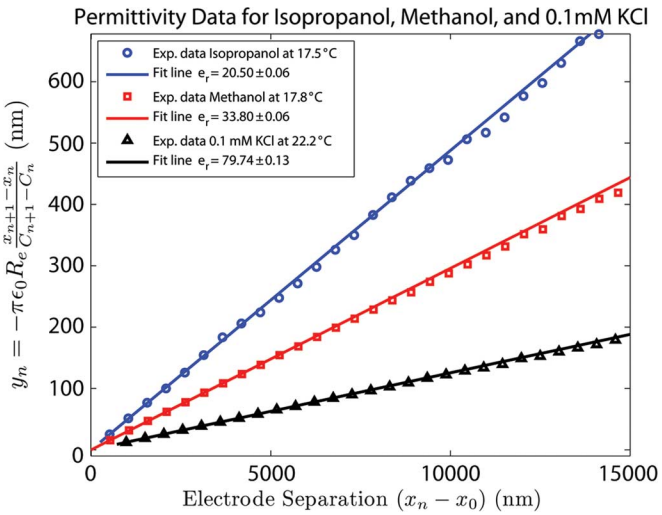

Fig. 9. The permittivity of methanol, isopropanol, and 0.1 mM KCl solution.

positive offset between the measured and the known ε_r value is a result of the presence of the electrode mounting shaft, which causes data points from larger electrode separations to droop downward in Fig. 8. This droop enlarges the measured permittivity by approximately 1% in the 1–10 μm electrode separation range.

Measured data for isopropanol, methanol, and water are plotted together in Fig. 9. A 0.1 mM KCl solution is used instead of deionized water in order to control the concentration of impurities at a stable level. The measurement parameters are exactly the same as nitrogen gas with the exception that the excitation amplitude is decreased to 10 mV RMS in order to prevent faradic reactions at the surface of the electrode. The measured data in these plots show significantly less noise than the data for nitrogen gas due to the higher permittivity values of these fluids. The measured ε_r for isopropanol at 17.5 °C, methanol at 17.8 °C, and a 0.1 mM KCl solution at 22.2 °C are 20.50 ± 0.06, 33.80 ± 0.06, and 79.74 ± 0.13 respectively. The established ε_r values for these substances at the specified temperatures are 20.62, 34.06, and 79.26 [15].

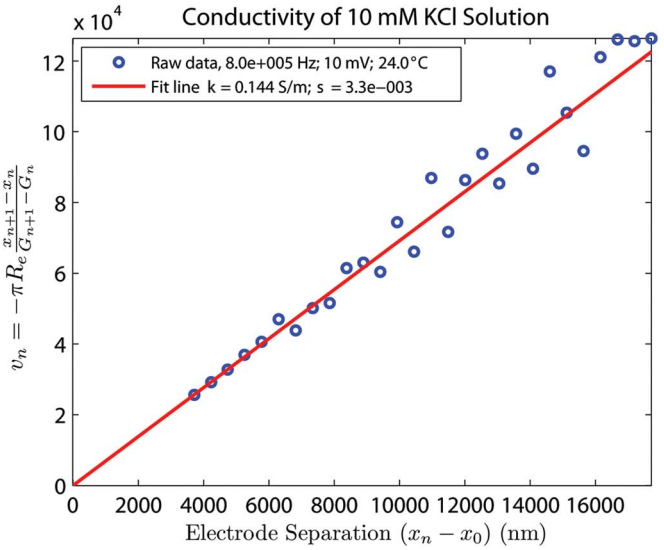

Fig. 10. Example data from conductivity of KCl solutions.

The repeatability of permittivity measurements has been studied using 30 repeated measurements of methanol at 17.7 °C. The mean of the measured ε_r is 34.5 with a standard deviation of 0.09. Once again, the measured values are approximately 1% greater than the known ε_r of 34.1 for methanol at 17.7 °C.

B. Electrical Conductivity Measurements

With each dataset, electrical conductivity data is collected simultaneously the electrical permittivity data. An example data set from electrical conductivity measurements of a 10 mM KCl solution is shown in Fig. 10. The measurements are made at 800 kHz, near the maximum frequency of the 4284A, while all other experimental conditions are identical to the permittivity measurements in Fig. 9. The conductivity results show more noise than the permittivity measurement because the measurement frequency is no longer the optimal measurement frequency described by the electrochemical model.

The conductivity of most solutions is approximately proportional to the molarity of ions in the solution. Therefore, conductivity measurements are more conveniently described using molar conductivity, Λ, defined as the electrical conductivity normalized over concentration c as

$$\Lambda = \kappa / c. \tag{4.1}$$

The variation of molar conductivities of KCl solutions can be predicted from Fuoss–Onsager theory [12] using

$$\Lambda = \Lambda_0 - Sc^{1/2} + Ec\log c + J_1 c - J_2 c^{3/2} \tag{4.2}$$

where Λ_0, S, E, J_1, J_2 are constants that must be measured to high accuracy by Barthel [12].

The molar conductivity of KCl solutions as a function of KCl molarity is shown in Fig. 11. Each data point represents the mean of approximately ten data sets, while the error bars indicate the standard deviation of that data set. The spread of the measured data largely fall within ±1% of the established value. Measurements using platinum electrodes showed a slow

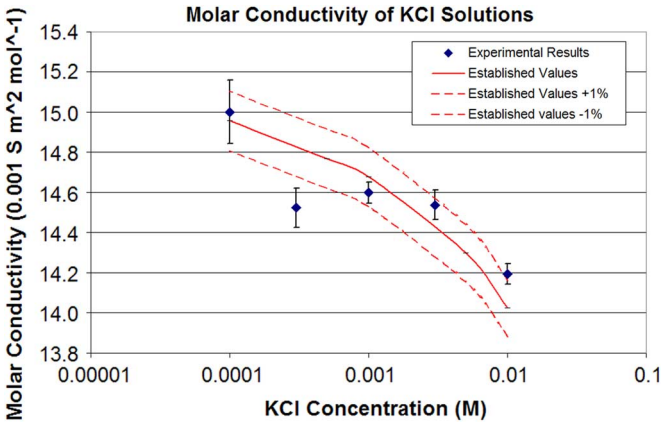

Fig. 11. Measured versus established molar conductivity of KCl solutions from 0.1 to 10 mM.

upward drift in the measured conductivity as a function of time. This drift error can be eliminated using ANSI-316 stainless steel spherical electrodes in place of the platinum electrodes. This behavior indicates that the slow increase in conductivity is caused by galvanic potentials established by platinum-stainless steel junction, which may oxidize the electrode and released free ions into the solution. While stainless steel electrodes provide sufficient diametrical accuracy for simple measurements, if the low surface roughness of silicon-nitride spheres is desired, the galvanic potential problem may be resolved by plating the electrode mounting shaft with a metal compatible with the metal deposited on the silicon-nitride spheres.

VI. Conclusion

A technique and device for measuring the bulk electrical permittivity and conductivity of liquids and gases without requiring prior calibration has been developed. The capability of this technique to measure electrical permittivity without requiring adjustment to the measurement apparatus or data analysis techniques was verified by measuring nitrogen gas, methanol, isopropanol, and water. The capability of this technique for measuring electrical conductivity was verified by measuring the conductivity of aqueous KCl solutions from mM to 10 mM. Results were primarily within $\pm 1\%$ of established values were obtained without adjustment of the apparatus or data analysis techniques.

Acknowledgment

The authors wish to thank D. R. Sadoway and A. J. Grodzinsky for insightful discussions, and K. Broderick and M. Belanger for assistance with design and fabrication.

References

[1] M. Tjahjono, T. Davis, and M. Garland, "Three-terminal capacitance cell for stopped-flow measurements of very dilute solutions," *Rev. Scientific Instrum.*, vol. 78, p. 023902, Feb. 2007.
[2] F. A. Wang, W. C. Wang, Y. L. Jiang, J. Q. Zhu, and J. C. Song, "A new model of dielectric constant for binary solutions," *Chem. Eng. Technol.*, vol. 23, pp. 623–627, Jul. 2000.
[3] M. Bittelli, M. Flury, and K. Roth, "Use of dielectric spectroscopy to estimate ice content in frozen porous media," *Water Resources Res.*, vol. 40, p. W04212, Apr. 22, 2004.
[4] W. Warsito and L. S. Fan, "Measurement of real-time flow structures in gas-liquid and gas-liquid-solid flow systems using electrical capacitance tomography (ECT)," *Chem. Eng. Sci.*, vol. 56, pp. 6455–6462, Nov. 2001.
[5] H. C. Yang, D. K. Kim, and M. H. Kim, "Void fraction measurement using impedance method," *Flow Meas. Instrum.*, vol. 14, pp. 151–160, Aug.–Oct. 2003.
[6] Y. C. Wu, W. F. Koch, and K. W. Pratt, "Low electrolytic conductivity standards," *J. Res. Nat. Inst. Standards Technol.*, vol. 100, pp. 191–201, 1991.
[7] J. K. Duchowski and H. Mannebach, "A novel approach to predictive maintenance: A portable, multi-component MEMS sensor for on-line monitoring of fluid condition in hydraulic and lubricating systems," *Tribology Trans.*, vol. 49, pp. 545–553, Oct.–Dec. 2006.
[8] S. L. Shiefelbein, N. A. Fried, K. G. Rhoads, and D. R. Sadoway, "A high-accuracy calibration-free technique for measuring the electrical conductivity of liquids," *Rev. Scientific Instrum.*, vol. 69, p. 3308, 1998.
[9] T. G. Drummond, M. G. Hill, and J. K. Barton, "Electrochemical DNA sensors," *Nature Biotechnol.*, vol. 21, pp. 1192–1199, Oct. 2003.
[10] I. Saad and J. M. Wallach, "Ethanal assay, using an enzymo-conductimetric method," *Anal. Lett.*, vol. 25, pp. 37–48, 1992.
[11] H. P. Schwan, "Linear and nonlinear electrode polarization and biological-materials," *Ann. Biomed. Eng.*, vol. 20, pp. 269–288, 1992.
[12] J. Barthel, F. Feuerlein, R. Neueder, and R. Wachter, "Calibration of conductance cells at various temperatures," *J. Solution Chem.*, vol. 9, pp. 209–219, 1980.
[13] J. Barthel, M. Krell, L. Iberl, and F. Feuerlein, "Conductance of 1-1 electrolytes in methanol solutions from −45-degrees-C to +25-degrees-C," *J. Electroanal. Chem.*, vol. 214, pp. 485–505, Dec. 10, 1986.
[14] Y. C. Wu, K. W. Pratt, and W. F. Koch, "Determination of the absolute specific conductance of primary standard KCl solutions," *J. Solution Chem.*, vol. 18, pp. 515–528, Jun. 1989.
[15] J. Barthel and R. Neueder, *Electrolyte Data Collection*. Frankfurt/Main, Germany: DECHEMA, 1992.
[16] P. Vanysek, "Equivalent conductivity of electrolytes in aqueous solution," in *CRC Handbook of Chemistry and Physics*, D. R. Lide, Ed., 87th ed. : CRC Press, 2007, pp. 5–75.
[17] J. R. White, H. Ma, J. Lang, and A. H. Slocum, "An instrument to control parallel plate separation for nanoscale flow control," *Rev. Scientific Instrum.*, vol. 74, p. 4869, Nov. 2003.
[18] J. P. Wu and J. P. W. Stark, "A high accuracy technique to measure the electrical conductivity of liquids using small test samples," *J. Appl. Phys.*, vol. 101, p. 054520, Mar. 2007.
[19] H. Ma, J. H. Lang, and A. H. Slocum, "Permittivity measurements using adjustable microscale electrode gaps between millimeter-sized spheres," *Rev. Scientific Instrum.*, vol. 79, p. 035105, 2008.
[20] H. Ma, "Electrochemical impedance spectroscopy using adjustable nanometer-gap electrodes," Ph.D. dissertation, Dept. Elect. Eng. Comput. Sci., Mass. Inst. Technol., Cambridge, MA, 2007.
[21] L. Boyer, F. Houze, A. Tonck, J. L. Loubet, and J. M. Georges, "The influence of surface-roughness on the capacitance between a sphere and a plane," *J. Phys. D-Appl. Phys.*, vol. 27, pp. 1504–1508, Jul. 14, 1994.
[22] A. J. Bard and L. R. Faulkner, *Electrochemical Methods: Fundamentals and Applications*. New York: Wiley, 2001.
[23] M. Z. Bazant, K. T. Chu, and B. J. Bayly, "Current-voltage relations for electrochemical thin films," *J. Appl. Math.*, vol. 65, pp. 1463–1484, 2005.
[24] A. H. Slocum, "Flexual bearings," in *Precision Machine Design*. Dearborn, MI: Society of Manufacturing Engineers, 1992, p. 521.
[25] *Agilent Technologies Impedance Measurement Handbook*. Santa Clara, CA: Agilent Technologies Co., Ltd., 2006.

Hongshen Ma (M'08) received the B.S. degree in engineering physics from the University of British Columbia (UBC), Vancouver, BC, Canada, in 2001, the M.S. degree from the Media Laboratory, Massachusetts Institute of Technology (MIT), Cambridge, in 2004, and the Ph.D. degree in electrical engineering from the Department of Electrical Engineering and Computer Science, MIT, in 2007.

He continued at MIT as a Postdoctoral Associate in the Department of Mechanical Engineering in 2008. He joined the faculty of UBC as an Assistant Professor in the Department of Mechanical Engineering in 2009. His current interests include sensor technologies, medical devices, and microelectromechanical systems.

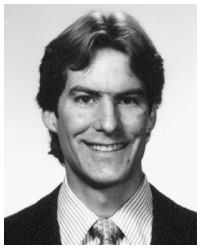

Jeffrey H. Lang (S'78–M'79–SM'95–F'98) received the B.S., M.S., and Ph.D. degrees from the Department of Electrical Engineering and Computer Science, Massachusetts Institute of Technology (MIT), Cambridge, in 1975, 1977, and 1980, respectively.

He joined the faculty of MIT in 1980, where he is now a Professor of Electrical Engineering and Computer Science. He served as the Associate Director of the MIT Laboratory for Electromagnetic and Electronic Systems between 1991 and 2003, and as an Associate Editor of Sensors and Actuators between 1991 and 1994. He is the coauthor of *Foundations of Analog and Digital Electronic Circuits* (Morgan Kaufman). His research and teaching interests focus on the analysis, design and control of electromechanical systems with an emphasis on rotating machinery, microscale (MEMS) sensors, actuators and energy converters, flexible structures, and the dual use of electromechanical actuators as motion and force sensors. He has written over 200 papers and holds 12 patents in the areas of electromechanics, MEMS, power electronics and applied control.

Prof. Lang has been awarded four best paper prizes from IEEE societies. He has also received two teaching awards from MIT. He is a former Hertz Foundation Fellow.

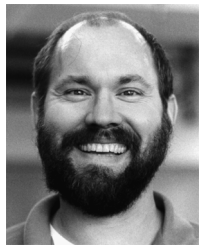

Alex H. Slocum is a Professor of Mechanical Engineering at the Massachusetts Institute of Technology (MIT), Cambridge, and a MacVicar Faculty Teaching Fellow. He has over five dozen patents issued/pending. His current interests focus on the development of precision machines and instruments, micro and nanotechnology, and medical devices.

Prof. Slocum has been involved with 11 products that have been awarded R&D 100 awards and is the recipient of the Society of Manufacturing Engineer's Frederick W. Taylor Research Medal, and the ASME Leonardo daVinci and Machine Design Award. He is a Fellow of the ASME.